
ELSEVIER

Nuclear Instruments and Methods in Physics Research B 164–165 (2000) 425–430

NIM B
Beam Interactions with Materials & Atoms

www.elsevier.nl/locate/nimb

Dose and implantation temperature influence on extended defects nucleation in c-Si

F. Schiettekatte, S. Roorda *, R. Poirier, M.O. Fortin, S. Chazal, R. Héliou

Groupe de recherche en science et technologie des couches minces et Département de physique, Université de Montréal, Montréal, Québec, Canada H3C 3J7

Abstract

We have investigated the effects of implantation temperature on the extended defect nucleation processes near the threshold dose where these defects appear after annealing. Defects induced by 230 keV P implantation were observed before and after annealing by means of channeling Rutherford backscattering spectroscopy (c-RBS), extended defect delineation etching (Wright etch) and transmission electron microscopy (TEM). It is revealed that the physical nature of the threshold is a steep increase of extended defect areal density, by 5–6 orders of magnitude, between 0.6×10^{14} and 2×10^{14} P/cm^2. The implantation temperature influences this density only at higher doses, for which higher temperatures contribute to reduce the number of extended defects. Second, c-RBS data before annealing show that the number of primary point defects is constant with dose at 300°C whereas it shows a linear dependence for room temperature implantation. This implies that the configuration of the point defects depends on dose and temperature, which strongly influences extended defect nucleation during subsequent annealing.

1. Introduction

Ion implantation produces point defects (PD) and PD complexes in Si. This phenomenon has been studied in depth over the last three decades [1] and the structure they adopt is well characterised both theoretically [2] and experimentally [3,4]. The induced PD can be removed by subsequent annealing. But when a certain threshold dose is reached, extended defects (XD) are observed after high temperature annealing [5]. Schreutelkamp et al. established that for room temperature implantation, the criterion for XD formation is the areal density of PD, whether the PD are distributed over a large depth or concentrated near the surface [6]. The XD structure and the way they interact with each other are also well characterised [7], since XD are observable in transmission electron microscope (TEM). This is not the case, however, for the defect structure during the transition between the as-implanted and the annealed regimes (>700°C) for which the situation is more obscure and often referred to as the 'missing link' [4,8]. For example, di-vacancy and vacancy-oxygen complexes are known to be stable [3] up to ~300°C. Above this

* Corresponding author. Tel.: +514-343-2076; fax: +514-343-6215.

E-mail address: sjoerd.roorda@umontreal.ca (S. Roorda).

0168-583X/00/$ - see front matter
PII: S0168-583X(99)01071-X

temperature, indirect measurements and simulations [9] suggest that PD clustering occurs and recently some experiments evidenced that these clusters ripen with increasing temperature to eventually form XD at high temperature [10].

Up to now, however, the effect of sample temperature on the XD nucleation process has only partially been explored [11]. Since it affects the dynamic recombination of PD during implantation, it will also greatly modify the following processes during subsequent annealing such as cluster formation and XD nucleation. This has technological implications on the implantation steps in the manufacturing process of very large scale integration (VLSI) silicon devices. For example, a high implantation current intensity can raise the wafer temperature and changes significantly the defect configuration [12]. This paper investigates the influence of the substrate temperature during implantation on the nucleation process of such XD for several doses near the threshold where they appear.

2. Experiment

The samples used for these experiments were ⟨1 0 0⟩ Czochralski (Cz) silicon wafers (undoped n type, $\rho \geqslant 10$ Ω cm, 300 μm thick). Phosphorus ions with an energy of 230 keV were implanted to 15 different doses ranging from 0.6×10^{14} to 5×10^{14} P/cm^2, with samples tilted at 7° angle with respect to surface normal in order to avoid channeling. The beam current was maintained approximately at 100 nA/cm^2 during the implantation. Each series of implantations were carried out at wafer temperatures of 23 ± 1, 150 ± 3 and 300 ± 2°C. For a given temperature, all the 12 implantation doses between 0.6×10^{14} and 2×10^{14} P/cm^2 were located on the same wafer. After implantation, the wafers were annealed in a rapid thermal annealing system (RTA, Minipulse, A.G. Associates) at 1000°C for 30 s (rise time 8 s, cooling time 10 s to 500°C) under N_2 atmosphere.

The density, size and configuration of the XD were determined by plan-view TEM carried out both in bright and dark field mode on a Philips CM-30 microscope operating at 300 kV. For samples with defect densities too low to be measurable at TEM ($<1.8 \times 10^{14}$ P/cm^2), the XD where delineated using a Wright etch solution [13] in order to measure their areal density by means of an optical microscope.

The areal density and position of PD in the as-implanted Si lattice as well as the dechanneling due to XD after annealing were measured by means of channeling Rutherford Backscattering Spectrometry (c-RBS) [14]. Both implantation and c-RBS spectra were obtained on the 1.7 MV Tandetron accelerator (HVEE) at the Université de Montréal.

3. Results and discussion

3.1. Point defects

The depth profile of scattering centres (PD) visible along the ⟨1 0 0⟩ direction by c-RBS in the as-implanted, 23°C samples is shown in Fig. 1(a) as a function of dose. The dechanneling component of each spectrum is deduced according to the '2-beam' (channeled–dechanneled beam components) method [14]. The remaining area, representing the contribution of the PD to the c-RBS spectrum, is reported on Fig. 1(b) for each dose.

For room temperature implantation, the density of PD in the ⟨1 0 0⟩ direction increases linearly, as expected, for doses up to 3×10^{14} P/cm^2. The PD density for a dose of 5×10^{14} P/cm^2 somewhat departs from linearity but the implanted layer is heavily damaged in this case as seen in Fig. 1(a). The PD density measured in the ⟨2 1 1⟩ direction is slightly lower, revealing some structure in the defects. When a dose $\geqslant 3 \times 10^{14}$ P/cm^2 is reached, the same yield is observed in both crystalline directions. This is the signature for the presence of amorphous clusters in the sample. With 'amorphous cluster' in this context we mean a complex defect structure, which has identical backscattering cross sections in ⟨2 1 1⟩ and ⟨1 0 0⟩ channeling directions. Since these amorphous clusters are already present at 3×10^{14} P/cm^2, they could capture more diffusing PD and thus slightly lower the dynamic recombination rate of Frenkel pairs, which

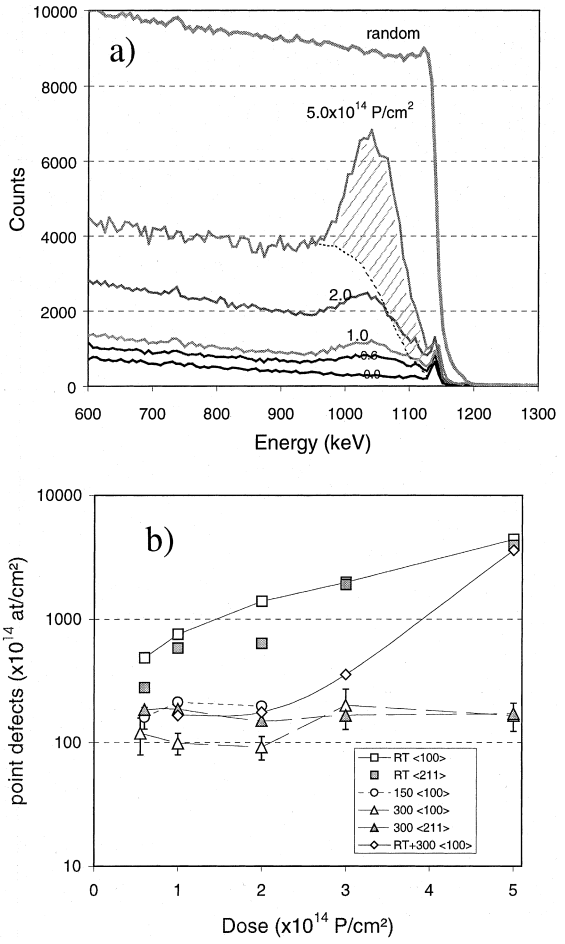

Fig. 1. (a) Progression of the channeling RBS spectrum in the $\langle 1\,0\,0\rangle$ direction with implanted dose at 23°C. The dotted line represents the dechanneling contribution to the spectrum. The integral of the hatched region, which is the density of scattering centres (PD) in this direction, is shown in (b) for several crystalline orientations and implantation temperatures.

explains the departure from linear increase in PD density at 5×10^{14} P/cm^2.

The amorphous signature, i.e. identical channeling in $\langle 1\,0\,0\rangle$ and $\langle 2\,1\,1\rangle$ directions, is also present above 2×10^{14} P/cm^2 in 300°C implants. But this time, two important aspects should be noticed. (1) The density of PD is stable with dose both for the 150°C and 300°C implantations, but the 150°C yields more than twice the number of PD as the 300°C implantation. This result, pointed out in an earlier work [15], is attributed to more effective PD recombination with increasing temperature. (2) For 300°C implantation below 3×10^{14} P/cm^2, the number of PD in the $\langle 1\,0\,0\rangle$ direction is about two times smaller than in the $\langle 2\,1\,1\rangle$ direction. This result suggests that PD surviving 300°C implantation occupy a site partially hidden by crystal atom columns in the $\langle 1\,0\,0\rangle$ direction and less hidden by crystal atoms in the $\langle 2\,1\,1\rangle$. A good candidate is thus an interstitial site near the $\frac{1}{2}\,\frac{1}{2}\,\frac{1}{2}$ position of the Si lattice. This is coherent with the di-interstitial structure deduced by Lee [4] from electron paramagnetic resonance (EPR) experiments which, he claims, are stable and constitute the building block for $\{3\,1\,1\}$ type XD. Surprisingly, for RT implants the $\langle 2\,1\,1\rangle$ direction scatters less than the $\langle 1\,0\,0\rangle$ direction, which would imply that the di-interstitial is not a dominant defect in RT implanted material.

In order to confirm that a hot implant is not the same as an implant followed by a hot anneal, the wafer implanted at room temperature was cleaved in two parts, one part being placed in the implantation chamber at 300°C for 1 h (which is about the implantation time for samples implanted at 300°C). The PD density along the $\langle 1\,0\,0\rangle$ is reported in Fig 1(b), labelled 'RT + 300 $\langle 1\,0\,0\rangle$'. While at low dose the areal density of PD is nearly two times the density found in samples implanted at 300°C, it increases progressively with dose to reach the level of PD in the unannealed sample. It is thus concluded that higher implantation temperatures affect the PD structure in a way significantly different than post-implantation annealing at the same temperature. Furthermore, amorphous clusters induced at room temperature by doses of 5×10^{14} P/cm^2 are sufficiently stable to resist post-implantation annealing at 300°C. If similar structures exist in samples implanted at 300°C at the same dose, they do not consist of more defects than at lower doses.

3.2. Extended defects: replacing '+1' by '$+n(T_{\text{implant}})$'

Samples were then annealed at 1000°C for 30 s in order to induce XD. This temperature is well above the dissolution temperature of $\{3\,1\,1\}$ XD [7]. Fig. 2 shows TEM micrographs of the

defects for room temperature and 300°C implantation. While a high areal density of small Frank loops is observed in the 23°C samples, a low density of large dislocation loops shows up for 300°C implants. The ratio of the number of interstitial atoms contained in these loops to the implanted dose is about 1.2 for 23°C implantation while for samples implanted at 300°C to doses of 2×10^{14} and 3×10^{14} P/cm^2 this ratio is 0.4. At 5×10^{14} P/cm^2 (more heavily damaged material) the ratio reaches +1.0 in this case. While our room temperature data compare quite well with data in the literature [5], showing a slight positive departure from the '+1' model, it is interesting to note the interstitial imbalance for higher temperature implantation. This suggests that significant deviations from the '+1' model not only depend on the ion mass [16], but also on the implant temperature, say '$+n(T_{\text{implant}})$'. It is not possible to state, however, if the 'missing' interstitial atoms have been lost during the implantation or the high temperature anneal, due to structural differences in XD precursors, for example.

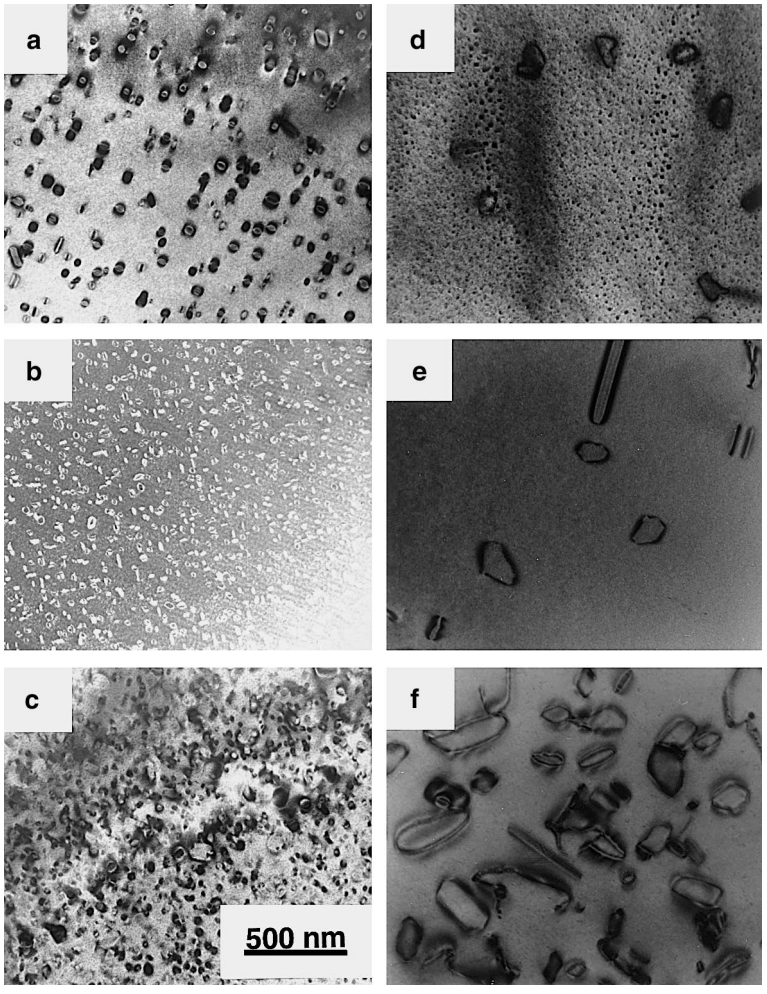

Fig. 2. TEM plan-view micrographs of samples implanted at 2.0×10^{14} (a, d), 3.0×10^{14} (b, e) and 5.0×10^{14} P/cm^2 (c, f) at implantation temperature of 23°C (a, b, c) and 300°C (d, e, f). All images in BF mode except (b), which is in DF mode.

3.3. Threshold: a steep increase

The XD densities observed in TEM, together with the XD areal density measured by Wright etch and the c-RBS step height, appear in Fig. 3. Fig. 3 can be divided in two parts. For lower doses, we observe a steep increase of the number of XD with dose (5 to 6 orders of magnitude between 0.6×10^{14} and 2×10^{14} P/cm^2). In this part, no noticeable difference is observed in the XD areal density below 1.7×10^{14} P/cm^2 between room temperature and 300°C implants. For higher doses, the XD density, which stabilises close to a linear increase, is lower by more than an order of magnitude for the 300°C implants compared to room temperature implants.

From these results, it can first be stated that the threshold dose is in fact a steep increase of the number of XD with dose in the lower dose region. A model, which discusses this XD density dependence on dose, will be presented in a separated paper [17]. There appears to be a mismatch between the TEM and Wright etch data, but this is due to saturation effects. For etched samples, the surface was saturated with etch pits for doses above 2.0×10^{14} P/cm^2 because of the high density of dislocations (see Wright etch upper detection limit level in Fig. 3). At least one TEM data point (1.5×10^{14} P/cm^2, 23°C) falls in the range of the Wright etch data.

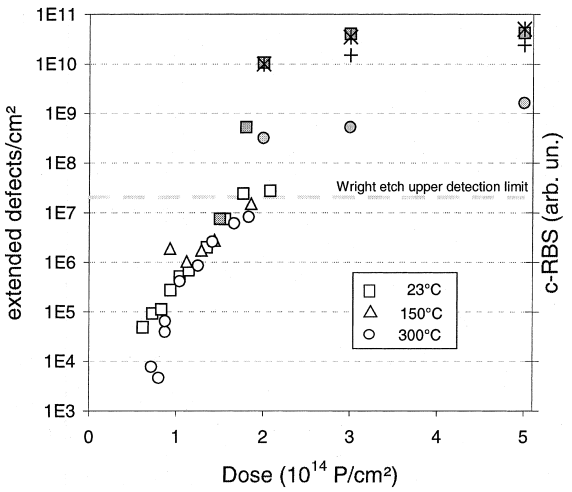

Fig. 3. Extended defect density in annealed samples measured by TEM (filled symbols) and revealed by Wright etch solution (open symbols). ∗ and + represent the dechanneling step heights in c-RBS spectrum for samples implanted at 23 and 300°C, respectively, the 23°C data being normalised to the corresponding TEM data.

As mentioned previously, Schreutelkamp et al. related the threshold dose to the density of point defects. When the data of Fig. 3 are compared with the PD density in Fig. 1(b), it can readily be stated that this criterion does not hold for implantation above room temperature, since the number of PD is quite stable with dose at 150°C and 300°C. These two features (steep increase of XD versus stability of PD) also imply a strong PD restructuring with increasing dose even if the number of PD is stable for implantation above room temperature.

It is interesting to note that the stabilisation of the XD density corresponds to doses where the 'amorphous cluster' signature is observed in as-implanted samples (Fig. 1(b)). It is thus tentatively concluded that XD have their origin in such amorphous clusters, which would act as nucleation sites. In this picture, the difference in the XD density at higher doses between 23°C and 300°C implantation would be explained by a saturation in the density of amorphous clusters that survive implantation at a given temperature. If the saturation density is smaller at higher implant temperatures, then the number of nucleation sites would be smaller, and, consequently, so would the XD density.

4. Summary

Ion implantation of 230 keV P to doses near the XD threshold have been performed in silicon samples for which the temperature was 23°C, 150°C and 300°C. The PD density measured by c-RBS shows that for all implant temperatures some structure exists at lower doses ($<2 \times 10^{14}$ P/cm^2) while an amorphous cluster signature is observed at higher doses. The low dose regime corresponds to a steep increase in XD density after high temperature anneal. The PD density being stable with dose above room temperature, the criterion [6]

relating the XD threshold to the areal density of PD does not hold above room temperature. It has also been concluded that amorphous clusters are the seeds for XD formation.

Acknowledgements

The authors are grateful to Pierre Bérichon and Réal Gosselin for technical assistance in the operation of the Tandetron accelerator at the Université de Montréal, as well as to Laurent Isnard for RTA operation. Special thanks also to Martin Chicoine for his advise about the TEM operation. This work benefited of grants from the Natural Science and Engineering Council of Canada and the Fonds pour la Formation des Chercheurs et d'Aide à la Recherche of Québec.

References

[1] J. Mayer, L. Erikson, J.A. Davies, Ion Implantation in Semiconductors, Academic Press, New York, 1970.
[2] M.J. Caturla, T.D. de la Rubia, G.H. Gilmer, Nucl. Instr. and Meth. B 106 (1995) 1.
[3] S.T. Pantelides, Deep Centers in Semiconductors, Gordon and Breach, New York, 1986.
[4] Y.H. Lee, Appl. Phys. Lett. 73 (8) (1998) 1119.
[5] P.A. Stolk, H.-J. Gossmann, D.J. Eaglesham, D.C. Jacobson, C.S. Rafferty, G.H. Gilmer, M. Jaraíz, J.M. Poate, H.S. Luftman, T.E. Haynes, J. Appl. Phys. 81 (9) (1997) 6031.
[6] R.J. Schreutelkamp, J.S. Custer, J.R. Liefting, W.X. Lu, F.W. Saris, Mater. Sci. Rep. 6 (1991) 275.
[7] J. Li, K.S. Jones, Appl. Phys. Lett. 73 (25) (1998) 3748.
[8] J.L. Benton, S. Libertino, P. Kringhøj, D.J. Eaglesham, J.M. Poate, S. Coffa, J. Appl. Phys. 82 (1) (1997) 120.
[9] M. Jaraíz, G.H. Gilmer, J.M. Poate, T.D. de la Rubia, Appl. Phys. Lett. 68 (3) (1996) 409.
[10] S. Libertino, S. Coffa, J.L. Benton, K. Halliburton, D.J. Eaglesham, Nucl. Instr. and Meth. B 148 (1999) 247.
[11] R. Liefting, Engineering of damage in ion implanted silicon, Thesis, University of Twente, 1992.
[12] R. Poirier, F. Schiettekatte, S. Roorda, M.O. Fortin, J. Vacuum Sci. and Techn. A, in press.
[13] M. Wright Jenkins, J. Electrochem. Soc. 124 (5) (1977) 757.
[14] M.L. Swanson, in: Handbook of Modern Ion Beam Materials Analysis, Material Research Society, 1995, Chapter 10.
[15] N. Hecking, K.F. Heidemann, E. te Kaat, Nucl. Instr. and Meth. B 15 (1986) 760.
[16] S.B. Herner, H.-J. Gossmann, L.P. Pelaz, G.H. Gilmer, M. Jaraíz, D.C. Jacobson, D.J. Eaglesham, J. Appl. Phys. 83 (11) (1998) 6182.
[17] F. Schiettekatte, S. Roorda, Unpublished.